Structure–Function Relationship Between Bruch's Membrane Opening–Based Optic Nerve Head Parameters and Visual Field Defects in Glaucoma

Daniel R. Muth and Christoph W. Hirneiß

Augenklinik der Ludwig-Maximilians-Universität München, Ludwig-Maximilians-University, Department of Ophthalmology, Klinikum der Universität München, Campus Innenstadt, Munich, Germany

Correspondence: Christoph Hirneiß, Augenklinik der Ludwig-Maximilians-Universität, Mathildenstr. 8, D-80336 München, Germany; Christoph.Hirneiss@med.uni-muenchen.de.

Submitted: October 10, 2014
Accepted: April 12, 2015

Citation: Muth DR, Hirneiß CW. Structure–function relationship between Bruch's membrane opening–based optic nerve head parameters and visual field defects in glaucoma. *Invest Ophthalmol Vis Sci.* 2015;56:3320–3328. DOI:10.1167/iovs.14-15845

Purpose. This study was performed to evaluate the structure–function relationship between Bruch's membrane opening (BMO) parameters of the optic nerve head (ONH) and visual field (VF) sensitivity.

Methods. Forty-six right eyes of 46 patients with open-angle glaucoma (OAG) in the patient group and 12 right eyes in the control group were included. Standard automated perimetry (SAP) and spectral-domain optical coherence tomography (SD-OCT) were assessed. Three BMO-based distances and two areas of the neuroretinal rim were used for correlation: the minimum rim width (MRW), the perpendicular rim width (PRW), the horizontal rim width (HRW), the minimum rim area (MRA) within the neuroretinal tissue defined by the MRW, and the perpendicular rim area (PRA) within the neuroretinal tissue defined by the PRW. These parameters were correlated with global and sectoral VF sensitivities. Spearman's correlation coefficients between BMO parameters and global and sectoral VF sensitivities were obtained.

Results. Within the patient group, significant correlations could be observed between global and sectoral VF sensitivities and BMO parameters, with PRW and PRA showing the highest values. In the sectoral analysis the highest correlations were found for the temporal–inferior VF sector (MD-TI): PRW-TI ($\rho = 0.72394$; $P < 0.00001$) and PRA-TI ($\rho = 0.77205$; $P < 0.00001$). Minimum rim width and MRA performed more weakly than PRW and PRA.

Conclusions. The BMO-based parameters PRW and PRA presented with a very good structure–function relationship in glaucoma patients, statistically at least equal to MRW and MRA. Using new BMO-based parameters might allow early objective assessments of functional glaucomatous impairments.

Keywords: glaucoma, spectral-domain optical coherence tomography, bruch membrane opening

Glaucoma is one of the major causes for blindness worldwide, with more than 60 million people affected.[1,2] In this progressive neuropathy of the optic nerve, characteristic functional visual field (VF) defects as well as structural changes of the optic nerve head (ONH) and the neuroretinal peripapillary nerve fiber layer (RNFL) occur.[3–5] Due to the irreversible nature of this disease, it is of vital importance to reliably detect the presence of glaucomatous changes as early as possible for adequate treatment. There is an ongoing discussion on whether structural defects precede functional impairments or vice versa.[2,3,6–10] It has been reported repeatedly that structural changes precede functional impairments in patients with early glaucoma,[7,10–14] but there have also been reports that structural and functional defects occur simultaneously.[3,15] However, techniques to measure structural changes have developed faster than functional tests.[9,14] A variety of techniques to measure the structural changes are now available: confocal scanning laser ophthalmoscopy (CSLO), scanning laser polarimetry (SLP), and spectral-domain optical coherence tomography (SD-OCT).[11,12,16,17] The visible part of the optic nerve, the optic nerve head (ONH), is routinely described for documentation of the structural glaucomatous damage.[18,19] Recent studies have found that this approach lacks accuracy for precisely estimating the neuroretinal rim tissue.[11,20,21] The reason is that the outer margin of the optic disc often does not exactly correspond with the outer margin of the neuroretinal rim tissue.[20,21]

Imaging of Bruch's membrane (BM) by SD-OCT is a new approach to precisely measure the anatomy of the ONH and RNFL. The outer border of the optic nerve is defined by the termination of BM around the optic nerve, forming a hole called the BM opening (BMO). This is the physiological opening for axons of the retinal ganglion cells (RGCs) to exit the globe.[18] Spectral-domain OCT imaging allows visualization and evaluation of the BM in high resolution.

This study was performed to evaluate several BMO-based parameters of the ONH in patients with open-angle glaucoma (OAG) and to correlate them with functional impairment assessed by standard automated perimetry (SAP).

Methods

Participants

This case–control study was conducted in a German university-affiliated glaucoma center: the glaucoma unit of the Depart-

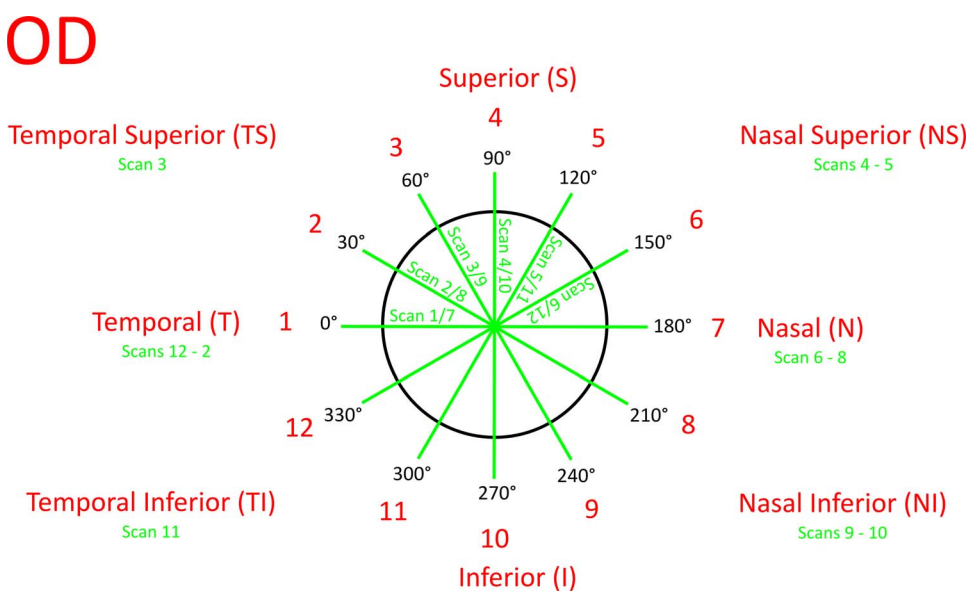

Figure 1. Assignment of SD-OCT scans to visual field sectors.

ment of Ophthalmology, Ludwig-Maximilians-University, Munich, Germany.

In the patient group as well as in the control group, the right eye of every enrolled participant was used for further analysis. All patients and control participants underwent a full ophthalmic examination, including slit-lamp biomicroscopy, intraocular pressure (IOP) measurement with Goldmann applanation tonometry, refraction, gonioscopy, dilated fundus examination by indirect ophthalmoscopy, and central corneal thickness (CCT) measurement.

Inclusion criteria for the patient group were clinical diagnosis of OAG, age > 18 years, a refractive error between −8 and +3 diopters, and a global mean deviation (MD-G) better than −20 dB. Glaucomatous eyes were defined as those with reliable abnormal SAP (at least three adjacent points had a ≥5 dB or at least one point had a ≥5 dB loss in compared numerical map) and optic nerve damage (rim thinning, notching, excavation, or retinal nerve fiber layer defect).

Patients not meeting the inclusion criteria were excluded from the study. Prior ocular surgery was not an exclusion criterion.

The patients' glaucoma stage was classified based on a simplified modification of the Hodapp-Anderson-Parrish system.[22,23] Patients were divided into three groups depending on their MD-G: early glaucoma (MD-G equal to or above −6 dB), moderate glaucoma (MD-G below −6 dB but equal to or above −12 dB), and severe glaucoma (MD-G below −12 dB). All included patients either were treated locally with antiglaucomatous medication or underwent glaucoma surgery to control the disease before SAP and SD-OCT measurements were done.

Inclusion criteria for the control group were no clinical diagnosis of OAG, no previous glaucoma surgery, age > 18 years, a refractive error between −8 and +3 diopters, a MD-G better than −4 dB, a normal SAP, and no glaucomatous optic nerve damage.

Participants who did not meet the inclusion criteria were excluded from the control group.

Ethical approval of the study was obtained from the Institutional Review Board (IRB) of the University Eye Hospital Munich in Germany, and all the patients who agreed to participate signed a consent form. The study adhered to the tenets of the Declaration of Helsinki.

Standard Automated Perimetry

Visual field sensitivity was assessed using the Humphrey Field Analyzer (HFA; Carl Zeiss Meditec AG, Jena, Germany) with the Swedish Interactive Threshold Algorithm (SITA) 24-2 standard algorithm. A reliable VF test was defined as having <25% rate of fixation losses and <20% false-positive and false-negative values. The VF testing had to have been done no more than 3 months prior to the SD-OCT examination.

Besides the MD-G and global pattern standard deviation (PSD-G), the HFA provides the VF sensitivities following a grid consisting of 54 test points that are distributed at a 6° distance from each other, covering approximately the central 24° of the VF.[24] The sensitivity values were recorded and analyzed in a logarithmic decibel scale. According to the structure–function map described by Garway-Heath et al.,[25] in 2002 the sensitivity values of the test points were summed up and average MD values were calculated for the respective VF sectors (MD-T, MD-TS, MD-NS, MD-N, MD-NI, MD-TI). These mean MD values were calculated based on the logarithmic decibel scale without previous conversion to a linear scale. The two fields of the 54-field grid representing the blind spot were excluded. The calculations were performed using Microsoft Excel (Microsoft Office 2003 for Windows; Microsoft Corporation, Redmond, WA, USA). The perimetrical data were processed and analyzed with the PeriData software for Windows, v3.0 (PeriData Software GmbH, Huerth, Germany).

Spectral-Domain Optical Coherence Tomography

Spectral-domain OCT images were recorded with a Heidelberg Spectralis device (Spectralis HRA&OCT, software version 5.2.0.3; Heidelberg Engineering, Heidelberg, Germany). A radial scan mode centered on the optic disc was used. Via active eye tracking technology, the Spectralis kept the measurement circle centered on the disc. The images were retrieved in high-speed (HS) mode. An automated real-time (ART) combination of nine records combined to one SD-OCT scan image was used to reduce signal noise.

Twelve scans per eye were performed dividing the optic disc into 30° segments, starting at a 0° position, which was defined as 9 o'clock temporal to the included right eyes. Figure 1 illustrates the assignment of the SD-OCT scans to the VF

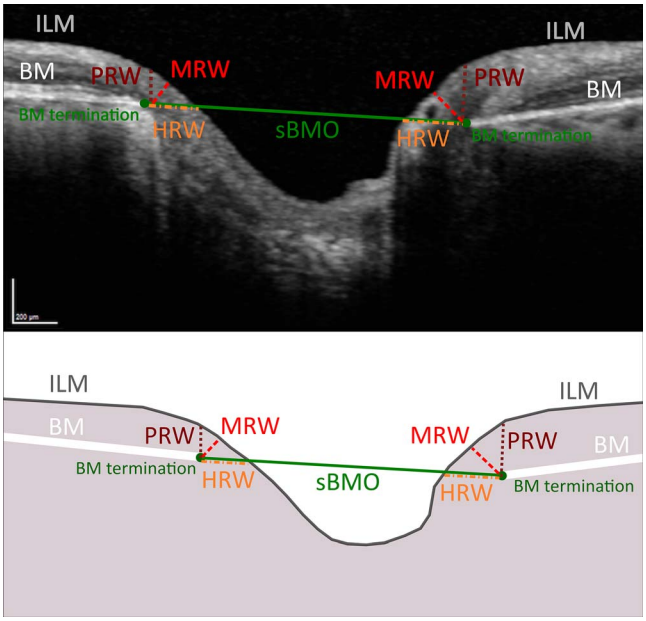

FIGURE 2. Bruch's membrane opening parameters. *Top*: Original OCT image with manual measurements done with the software ImageJ. *Bottom*: Schematic illustration of measurements: internal limiting membrane (ILM; *continuous gray line*), Bruch's membrane (BM), Bruch's membrane termination (BM termination; *dot*), connection line between two BM terminations (sBMO; *continuous black line*), minimum rim width (MRW; *dashed line*), perpendicular rim width (PRW; *dotted line*), horizontal rim width (HRW; *dashed-dotted line*).

sectors in right eye format. The signal of the SD-OCT examination had to be at least 15 dB to be included in the study, a commonly used cutoff level for obtained scans.

The images were exported to the Heidelberg Eye Explorer software for Windows, v1.7.1.0 (HRA/Spectralis viewing module v5.6.1.0; Heidelberg Engineering).

Bruch's Membrane Opening Parameters

For generating the SD-OCT–assessed BMO parameters of the ONH, the SD-OCT images were exported from the Heidelberg Eye Explorer as a standardized screen shot with scale 1:1 μm and zoom 400% for manual measuring. This allowed maximal preservation of contrast and image resolution. All images were processed by one examiner (DRM). The examiner was masked to the VF results at the time of grading. The screen shots were imported to the open source software ImageJ for Windows, v. 1.46r (http://imagej.nih.gov/ij/; provided in the public domain by the National Institutes of Health, Bethesda, MD, USA). ImageJ was used to precisely measure distances in pixels. Since all the processed screen shot images included a reference scale, the measured distances could be converted into micrometers (μm).

A total of four BMO-based distances of the ONH were defined (Fig. 2). No automated delineation was used. First, the two opposing terminations of BM were determined and a line was drawn connecting these two points. The distance between the opposing terminations as part of this line was defined as sectoral Bruch's membrane opening (sBMO). The sBMO was determined for each scan. The part of the sBMO ranging from BM termination to the point of intersection with the internal limiting membrane (ILM) was defined as the horizontal rim width (HRW). The distance between the BM termination and the ILM on a line perpendicular to the sBMO (going through BM termination) was defined as the perpendicular rim width (PRW). The shortest distance on any line through the BM termination between the BM termination and the point of intersection with the ILM was defined as the minimum rim width (MRW). The basic principle of determining the MRW was to place a circle centered at the BM termination points and resizing it until it just touched the ILM. The radius of this circle then equals the MRW. Minimum rim width, PRW, and HRW were used for further analysis.

A simple individual three-dimensional model of the neuroretinal rim of the ONH was created using MRW, PRW, HRW, and other measured widths (Supplementary Fig. S1). For this purpose, the computer-aided design (CAD) software Pro/ENGINEER Wildfire 4.0 for Windows was used (PTC; Needham, MA, USA). Within this three-dimensional model, two BMO-based areas were calculated with the CAD software: (1) MRA as the area within the neuroretinal rim defined by MRW between two neighboring SD-OCT radial scans and (2) PRA as the area within the neuroretinal rim defined by PRW between two neighboring SD-OCT radial scans.

Statistical Analysis

Descriptive statistical analyses were performed to characterize the patients' clinical, functional, and structural data. The Kolmogorov-Smirnov test was used for testing on normal distribution. As most of the measured parameters were not normally distributed and the data set showed an interval scale of measurement, Spearman's rank correlation analysis was used and a correlation coefficient ρ was obtained. Correlations were calculated for the patient group and the control group between the BMO-based parameters (in micrometers and square micrometers, respectively) and the global as well as the sectoral VF (in decibels). Before averaging of the VF values, they were converted to a linear scale. 1/Lambert was chosen as linear scale as it is used in the literature.[11] The following formula was used: $\mathrm{dB} = 10 \times log_{10}\left(\frac{1}{\mathrm{Lambert}}\right)$.

The average VF sensitivity values for each sector having been calculated, the values were reconverted to the logarithmic decibel scale.

The type 1 error, alpha (α), was defined as $\alpha = 0.05$, implying that the level of statistical significance was at 0.05. Therefore, the probability value (P) had to be equal to or smaller than 0.05 to assume statistical significance ($P \leq 0.05$).

Within the patient group, a significant difference between the correlations ρ(MRW and respective MD) and ρ(PRW and respective MD) was quantified by a two-tailed Williams t-test (version 1959) for two dependent groups with overlapping correlations.[26,27] It was performed using the online tool on the website http://comparingcorrelations.org/ (in the public domain).[28] The same was done within the patient group for the area correlations ρ(PRA and respective MD) and ρ(MRA and respective MD).

To account for the intrarater reliability of measuring MRW, PRW, and HRW, these distances were measured twice within the control group by the same examiner (DRM), resulting in MRWcontrol 1, MRWcontrol 2, PRWcontrol 1, PRWcontrol 2, HRWcontrol 1, and HRWcontrol 2. A Bland-Altman plot for each of the measurement pairs was computed to statistically evaluate the reproducibility of these measurements (Supplementary Fig. S2). If not stated otherwise, all statistical analyses were conducted using the software SPSS for Windows, v21.0 (IBM Corporation, Armonk, NY, USA).

RESULTS

Forty-six right eyes of 46 patients were enrolled in the patient group. Patients' characteristics are displayed in Table 1.

Table 1. Characteristics of Patient Group and Control Group

	Patient Group	Control Group
No. of patients (no. of eyes)	46 (46)	12 (12)
Age, y, arithmetic mean ± SD [95% CI]; median	63.4 ± 12.8 [59.6 to 67.2]; 66.5	44.1 ± 17.9 [27.6 to 60.7]; 53.0
Sex ratio, male/female	18/28	5/7
MD-G, dB, arithmetic mean ± SD [95% CI]	−5.8 ± 6.3 [−7.7 to −4.0]	−1.3 ± 1.5 [−2.8 to 0.1]
PSD-G, dB, arithmetic mean ± SD [95% CI]	5.3 ± 3.9 [4.2 to 6.5]	1.7 ± 0.3 [1.4 to 2.0]
Refraction:		
Sphere, D, arithmetic mean ± SD	−0.8 ± 2.7	0.8 ± 2.1
Cylinder, D, arithmetic mean ± SD	−0.8 ± 0.6	−0.7 ± 0.6
IOP, mm Hg, arithmetic mean ± SD	14.3 ± 3.7	13.5 ± 3.9

SD, standard deviation; MD-G, global visual field mean deviation; PSD-G, global visual field pattern standard deviation; D, diopter; 95% CI, 95% confidence interval.

According to the simplified modification of the Hodapp-Anderson-Parrish classification, 30 of 46 (65.2%) of the study participants could be allocated to the early glaucoma group, 8 of 46 (17.4%) to the moderate glaucoma group, and 8 of 46 (17.4%) to the severe glaucoma group.

Twelve participants were enrolled in the control group; these participants' characteristics are also displayed in Table 1.

Distances

Within the patient group, the BMO-based ONH parameters MRW, PRW, and HRW were significantly correlated with global and sectoral VF sensitivities (Tables 2–4). Perpendicular rim width values and MRW values showed a stronger correlation with functional data than HRW values. Perpendicular rim width revealed slightly higher coefficients than MRW. Within the TI sector, the Williams *t*-test showed a significantly higher correlation of PRW compared to MRW. For the other sectors, the differences between the correlations ρ(MRW and respective MD) and ρ(PRW and respective MD) were not significant for $P < 0.05$ (Supplementary Table S1).

Perpendicular rim width showed its highest sectoral correlation with the temporal–inferior VF sector (PRW-TI and MD-TI: $\rho = 0.72394$; $P < 0.00001$). This sector was also best for HRW (HRW-TI and MD-TI: $\rho = 0.49903$; $P < 0.00042$). The highest sectoral correlation of MRW was found in the temporal–superior sector (MRW-TS and MD-TS: $\rho = 0.59188$; $P < 0.00001$). Regarding the VF sectors, MD-TI, MD-NI, and MD-TS correlated best. All BMO-based distances had the lowest correlations with MD-N.

The best overall Spearman's correlation of a BMO-based distance was between PRW-TS and MD-G ($\rho = 0.75239$; $P < 0.00001$). The scatter plots in the Supplementary Figures S3 and S4 visualize these relationships.

Within the control group, no distance showed a statistically significant correlation with its respective VF sensitivity (Supplementary Tables S2–S4).

Areas

Both investigated areas, MRA and PRA, revealed significant correlation coefficients with the global as well as the sectoral VF sensitivities (Tables 5, 6) within the patient group. Perpendicular rim area showed higher sectoral correlations than MRA for every tested VF sector. However, the sectoral correlations were not significantly different for $P < 0.05$ according to the Williams *t*-test (Supplementary Table S5). Regarding MD-G, all PRA areas outperformed MRA. Only when correlated with PSD-G, the areas MRA-N, MRA-NI, and MRA-TI showed slightly better results than the respective PRA areas.

The highest coefficients were observed between the MD-TI sector and the areas MRA-TI ($\rho = 0.73788$; $P < 0.00001$) and PRA-TI ($\rho = 0.77205$; $P < 0.00001$) (Supplementary Figs. S5, S6). MD-TI had the best and MD-N the weakest correlation with the corresponding areas.

The control group showed two statistically significant correlations of an area and its respective VF sensitivity on a $P < 0.05$ level: MD-T and PRA-T ($\rho = 0.82857$; $P = 0.04156$) and MD-N and PRA-N ($\rho = 0.82857$; $P = 0.04156$) (Supplementary Tables S6, S7).

Discussion

With the evolution of high-speed and high-resolution imaging devices over the last years, especially SD-OCT, many studies on the structure–function relationship in glaucomatous eyes have been conducted.[8,11,12,24,29–32] The structural parameters most commonly investigated are the RNFL thickness, usually assessed by SPL and OCT, and ONH parameters, commonly measured by CSLO. A few years ago, OCT technology improved tremendously, and all structural parameters of interest can be measured in high resolution with a single device.[8,24,31,32]

Recently, Nilforushan et al.[11] compared SD-OCT-assessed rim area with VF sensitivity (SAP 24-2) and found an R^2 of 0.26 in the TI sector. Bowd et al.[8] investigated the same parameters but assessed rim area with CSLO. Their strongest relation could also be found within the TI sector: $R^2 = 0.25$. Reus and Lemij[9] found their best correlation between rim area (CSLO) and VF (SAP 24-2) within the TS sector: $r = 0.75$. The same group investigated the correlation between SLP-assessed RNFL thickness and VF sensitivity (SAP 24-2).[33] They found a correlation coefficient of $r = 0.77$ within the TS sector. Bowd et al.[8] and Leite et al.[31] both used SD-OCT to acquire RNFL thickness and compared it to VF measurements (SAP 24-2). They provided a $R^2 = 0.38$ (TI sector) and $R^2 = 0.31$ (TS sector), respectively. Pollet-Villard et al.[17] found a logarithmic regression coefficient R^2 of 0.658 between an SD-OCT-assessed MRW in the TI sector and the corresponding VF sector.

The cited results give a rough overview of correlations and relationships of different structural measurement methods and depict a predominantly moderate relationship between structural and functional changes in glaucoma patients. However, it is difficult to compare the results of these studies because different measurement techniques were used, inhomogeneous patient populations were enrolled (glaucoma patients, mixed glaucoma and healthy patients, patients of different descent, different MD ranges, and so on), different definitions of VF sectors were presented, and different scales and different statistical methods were used to analyze the data. Additional

Investigative Ophthalmology & Visual Science

TABLE 2. Spearman's Correlation (ρ) in Patient Group Between MRW and PSD-G and MD-G and Sectoral MDs ($\alpha = 0.05$; $P \leq 0.05$)

	MRW-T		MRW-TS		MRW-NS		MRW-N		MRW-NI		MRW-TI		MRW-G	
	ρ	*P*	ρ	*P*	ρ	*P*	ρ	*P*	ρ	*P*	ρ	*P*	ρ	*P*
PSD-G	**−0.39664**	0.00635	**−0.52489**	0.00018	−0.28056	0.05895	**−0.35671**	0.01496	**−0.68806**	<0.00000	**−0.58432**	0.00002	**−0.65967**	<0.00000
MD-G	**0.40022**	0.00585	**0.61409**	0.00001	**0.34477**	0.01896	**0.46154**	0.00124	**0.62667**	<0.00000	**0.51150**	0.00028	**0.68873**	<0.00000
MD-T	**0.51004**	0.00029	**0.56018**	0.00005	**0.37904**	0.00938	**0.36332**	0.01307	**0.59724**	0.00001	**0.52885**	0.00016	**0.66323**	<0.00000
MD-TS	**0.40026**	0.00585	**0.59188**	0.00001	0.33020	0.02502	**0.34919**	0.01738	**0.47865**	0.00077	**0.47310**	0.00090	**0.59953**	0.00001
MD-NS	**0.44718**	0.00183	**0.53623**	0.00012	**0.34616**	0.01845	**0.37416**	0.01042	**0.35430**	0.01570	**0.39044**	0.00730	**0.54055**	0.00011
MD-N	0.24234	0.10465	**0.33807**	0.02157	0.21255	0.15614	0.27732	0.06206	0.25998	0.08100	0.25468	0.08762	**0.35288**	0.01615
MD-NI	**0.35368**	0.01590	**0.46741**	0.00106	**0.37243**	0.01081	**0.41647**	0.00399	**0.58767**	0.00002	**0.47974**	0.00074	**0.61838**	<0.00000
MD-TI	**0.31843**	0.03103	**0.40021**	0.00585	**0.31195**	0.03481	**0.36166**	0.01352	**0.71136**	<0.00000	**0.55125**	0.00007	**0.62051**	<0.00000

PSD/PSD-G, pattern standard deviation/global PSD; MD/MD-G, mean deviation/global MD; MRW, mean value of minimum rim width. Bold indicates $P < 0.05$.

care is advisable in terms of precision of the structural measurements. It is technically not yet possible to selectively measure the exact number of functioning RGCs and their axons. Consequently, all existing structural measures are mere estimates of the number of working RGCs.[19] Chauhan et al.[18,21] and Reis et al.[20] found that estimates not based on BMO parameters might be anatomically incorrect or at least based on an inaccurate fundament, as the often used clinically visible disc margin does not necessarily represent the true anatomic border of the neuroretinal rim.

Therefore, in this study, the BMO was used as reference for assessing parameters that are anatomically as precise as possible. It is striking that with this approach the correlation results in this study were considerably different from results obtained by other measurement methods. As the correlation results of this study predominantly show higher values compared to results found in the literature, it seems that BMO-based structural measurements are a reasonable advancement in the structure–function research in glaucoma patients. It remains to be seen if future studies can confirm this approach by providing comparably high correlation results. The results of Pollet-Villard et al.,[17] for instance, are very promising in this respect.[17]

Using the MRW, the RGC axons should be cut almost vertically in theory. Consequently, MRW is independent of a reference line such as BMO. It needs only the termination of BM as a starting point. This means that MRW always cuts the nerve fibers at the same angle (ideally 90°), independently of their course through the ONH.[17] In contrast, a distance that is dependent on the BMO, like HRW and PRW, is always constructed at a fixed angle toward BMO and does not respect the actual variability of the optic nerve fibers. Therefore, MRW is supposed to be the most accurate thickness measurement of the neuroretinal rim.[12,18,19] However, in the present study PRW, a BMO-based parameter dependent on BMO as reference, revealed the highest correlation values with VF sensitivities (Tables 2–4). With performance of a Williams *t*-test, PRW proved to be as least as highly correlated with respective sectoral MD as MRW. Within the TI VF sector, which is the sector that usually shows the first changes in early glaucoma,[34] PRW correlated significantly more highly with MD-TI than MRW-TI (Supplementary Tables S1, S2). At the same time, PRW allows a more standardized geometric construction. This robustness is especially helpful in low-quality images, as these may occur in clinical practice far more often than in a hand-picked study population. This makes PRW a well-correlated and highly reproducible addendum or even alternative to MRW.

The reason why HRW, which can be constructed reproducibly too, correlates more weakly than MRW and PRW might be the angle at which HRW intersects the nerve fibers. This angle might be less sensitive to nerve fiber loss. Horizontal rim width might therefore be influenced more by supportive tissue like glia cells and blood vessels.[3]

The highest coefficients could be found when the areas MRA and PRA were correlated. For the global VF parameters (MD-G and PSD-G), the BMO-based areas achieved higher correlations for almost every structural sector than the BMO-based distances. However, with regard to the single VF sectors, a less clear image appeared: The sectoral areas scored better only in MD-T and MD-TI and MD-NI for PRA. In the other sectors, the distance PRW scored higher, except in MD-NI where MRW showed the strongest correlation. In order to calculate the areas the software used the measured distances. As the distances are squared in order to provide an area, measurement errors of the distances are squared, too. Therefore, the areas are influenced more by measurement errors than the distances, which might be an explanation for this finding.

Table 3. Spearman's Correlation (ρ) in Patient Group Between PRW and PSD-G and MD-G and Sectoral MDs ($\alpha = 0.05$; $P \leq 0.05$)

	PRW-T		PRW-TS		PRW-NS		PRW-N		PRW-NI		PRW-TI		PRW-G	
	ρ	P	ρ	P	ρ	P	ρ	P	ρ	P	ρ	P	ρ	P
PSD-G	**−0.43910**	0.00227	**−0.62178**	<0.00000	**−0.34301**	0.01961	−0.28698	0.05315	**−0.60049**	0.00001	**−0.65202**	<0.00000	**−0.65411**	<0.00000
MD-G	**0.47295**	0.00090	**0.75239**	<0.00000	**0.44754**	0.00182	**0.45395**	0.00153	**0.60132**	0.00001	**0.60854**	0.00001	**0.73773**	<0.00000
MD-T	**0.57393**	0.00003	**0.64819**	<0.00000	**0.44516**	0.00194	**0.35277**	0.01619	**0.49770**	0.00043	**0.61735**	<0.00000	**0.68441**	<0.00000
MD-TS	**0.50473**	0.00035	**0.71233**	<0.00000	**0.43948**	0.00224	**0.35012**	0.01706	**0.38034**	0.00912	**0.58034**	0.00002	**0.65795**	<0.00000
MD-NS	**0.47777**	0.00079	**0.66932**	<0.00000	**0.46334**	0.00118	**0.44755**	0.00182	0.26056	0.08030	**0.44447**	0.00197	**0.60310**	0.00001
MD-N	**0.35078**	0.01684	**0.56549**	0.00004	**0.32839**	0.02587	**0.37231**	0.01084	0.21095	0.15936	**0.33536**	0.02271	**0.45577**	0.00146
MD-NI	**0.48307**	0.00067	**0.73383**	<0.00000	**0.40944**	0.00472	**0.47653**	0.00081	**0.55843**	0.00006	**0.60666**	0.00001	**0.72293**	<0.00000
MD-TI	**0.40150**	0.00568	**0.65598**	<0.00000	**0.34069**	0.02051	**0.34483**	0.01893	**0.64845**	<0.00000	**0.72394**	<0.00000	**0.68048**	<0.00000

PRW, mean value of perpendicular rim width. Bold indicates $P < 0.05$.

Table 4. Spearman's Correlation (ρ) in Patient Group Between HRW and PSD-G and MD-G and Sectoral MDs ($\alpha = 0.05$; $P \leq 0.05$)

	HRW-T		HRW-TS		HRW-NS		HRW-N		HRW-NI		HRW-TI		HRW-G	
	ρ	P	ρ	P	ρ	P	ρ	P	ρ	P	ρ	P	ρ	P
PSD-G	−0.26173	0.07890	**−0.48798**	0.00058	−0.27788	0.06151	**−0.31141**	0.03514	**−0.60191**	0.00001	**−0.57514**	0.00003	**−0.62598**	<0.00000
MD-G	0.22016	0.14151	**0.54845**	0.00008	**0.29142**	0.04942	**0.39066**	0.00727	**0.53297**	0.00014	**0.50440**	0.00035	**0.62649**	<0.00000
MD-T	**0.32409**	0.02800	**0.47316**	0.00090	**0.34199**	0.02000	**0.32520**	0.02744	**0.52379**	0.00019	**0.50894**	0.00030	**0.61951**	<0.00000
MD-TS	0.19569	0.19246	**0.48740**	0.00059	0.27341	0.06599	**0.32693**	0.02658	**0.44553**	0.00192	**0.42957**	0.00289	**0.54605**	0.00009
MD-NS	0.26451	0.07567	**0.43978**	0.00223	0.27747	0.06191	0.29127	0.04953	**0.31903**	0.03069	**0.37232**	0.01083	**0.49911**	0.00041
MD-N	0.09203	0.54300	0.25289	0.08995	0.14298	0.34316	0.17863	0.23493	0.19318	0.19833	0.21071	0.15984	0.28305	0.05664
MD-NI	0.14709	0.32934	**0.35553**	0.01532	**0.32940**	0.02539	**0.35245**	0.01629	**0.47481**	0.00086	**0.42302**	0.00340	**0.54955**	0.00008
MD-TI	0.17343	0.24905	**0.30498**	0.03931	0.30604	0.03860	**0.31602**	0.03239	**0.60941**	0.00001	**0.49903**	0.00042	**0.56871**	0.00004

HRW, mean value of horizontal rim width. Bold indicates $P < 0.05$.

Table 5. Spearman's Correlation (ρ) in Patient Group Between MRA and PSD-G and MD-G and Sectoral MDs ($\alpha = 0.05$; $P \leq 0.05$)

	MRA-T		MRA-TS		MRA-NS		MRA-N		MRA-NI		MRA-TI		MRA-G	
	ρ	*P*	ρ	*P*	ρ	*P*	ρ	*P*	ρ	*P*	ρ	*P*	ρ	*P*
PSD-G	**−0.57987**	0.00002	**−0.59691**	0.00001	**−0.30043**	0.04249	**−0.46737**	0.00106	**−0.66874**	<0.00000	**−0.74188**	<0.00000	**−0.68967**	<0.00000
MD-G	**0.53846**	0.00011	**0.62809**	<0.00000	**0.32780**	0.02615	**0.54222**	0.00010	**0.57924**	0.00002	**0.64086**	<0.00000	**0.66183**	<0.00000
MD-T	**0.60538**	0.00001	**0.58812**	0.00002	**0.37312**	0.01065	**0.47273**	0.00091	**0.57535**	0.00003	**0.64615**	<0.00000	**0.66755**	<0.00000
MD-TS	**0.49813**	0.00043	**0.58620**	0.00002	**0.32249**	0.02883	**0.41259**	0.00438	**0.46107**	0.00126	**0.52990**	0.00015	**0.57399**	0.00003
MD-NS	**0.49393**	0.00049	**0.50897**	0.00030	**0.31878**	0.03083	**0.42522**	0.00322	**0.32741**	0.02634	**0.42670**	0.00310	**0.51489**	0.00025
MD-N	**0.30902**	0.03665	**0.30729**	0.03777	0.17264	0.25124	**0.27682**	0.06254	0.20638	0.16879	0.28996	0.05062	**0.33345**	0.02354
MD-NI	**0.46753**	0.00105	**0.54067**	0.00010	**0.39624**	0.00641	**0.49726**	0.00044	**0.56990**	0.00004	**0.61431**	0.00001	**0.64391**	0.00000
MD-TI	**0.48526**	0.00063	**0.47823**	0.00078	**0.35630**	0.01508	**0.47305**	0.00090	**0.67577**	<0.00000	**0.73788**	<0.00000	**0.67004**	<0.00000

MRA, mean value of minimum rim area. Bold indicates $P < 0.05$.

Table 6. Spearman's Correlation (ρ) in Patient Group Between PRA and PSD-G and MD-G and Sectoral MDs ($\alpha = 0.05$; $P \leq 0.05$)

	PRA-T		PRA-TS		PRA-NS		PRA-N		PRA-NI		PRA-TI		PRA-G	
	ρ	*P*	ρ	*P*	ρ	*P*	ρ	*P*	ρ	*P*	ρ	*P*	ρ	*P*
PSD-G	**−0.60734**	0.00001	**−0.67405**	<0.00000	**−0.42400**	0.00332	**−0.43503**	0.00252	**−0.63431**	<0.00000	**−0.73731**	<0.00000	**−0.70763**	<0.00000
MD-G	**0.60533**	0.00001	**0.71032**	<0.00000	**0.47512**	0.00085	**0.54519**	0.00009	**0.60416**	0.00001	**0.66769**	<0.00000	**0.73018**	<0.00000
MD-T	**0.64757**	<0.00000	**0.65404**	<0.00000	**0.47175**	0.00093	**0.47057**	0.00097	**0.51331**	0.00026	**0.63141**	<0.00000	**0.67699**	<0.00000
MD-TS	**0.56610**	0.00004	**0.66471**	<0.00000	**0.46614**	0.00109	**0.40926**	0.00474	**0.39576**	0.00648	**0.51306**	0.00027	**0.61982**	<0.00000
MD-NS	**0.52797**	0.00016	**0.58841**	0.00002	**0.44954**	0.00172	**0.45988**	0.00130	0.28733	0.05285	**0.41252**	0.00439	**0.56078**	0.00005
MD-N	**0.37946**	0.00930	**0.43534**	0.00250	0.28019	0.05929	**0.33388**	0.02335	0.21693	0.14758	**0.30544**	0.03900	**0.41524**	0.00411
MD-NI	**0.60456**	0.00001	**0.67314**	<0.00000	**0.47476**	0.00086	**0.53130**	0.00015	**0.59593**	0.00001	**0.66007**	<0.00000	**0.73124**	<0.00000
MD-TI	**0.58197**	0.00002	**0.62113**	<0.00000	**0.41984**	0.00368	**0.45054**	0.00168	**0.67442**	<0.00000	**0.77205**	<0.00000	**0.71420**	<0.00000

PRA, mean value of perpendicular rim area. Bold indicates $P < 0.05$.

Within the control group, none of the distances and only two areas (PRA-T and PRA-N) correlated statistically significantly with their respective VF sensitivities, which suggests that the observed structure–function relationship found within the patient group is glaucoma-associated.

This study establishes two new structural parameters, PRW and PRA, which correlate equally or significantly more highly with their respective MD than MRW and MRA. Furthermore, it could be shown that HRW does not correlate as well as MRW and PRW.

This study had some limitations. Since the manual measurement of the BMO parameters is complex and very time-consuming, the study was based on a rather small sample size of 46 eyes in the patient group and 12 eyes in the control group. The measurements in this study were performed by one person (DRM). Consequently, examiner bias cannot be excluded.

In addition, the SD-OCT quality of the images used for this study was not perfect for every single sector.

The generated three-dimensional model was based on the two-dimensional measurement data retrieved from the SD-OCT scans. As there were only 12 scans per eye available, a sector between two scans was 30° wide. This implies that the CAD software used had to interpolate the data between two scans in order to build the three-dimensional model. Consequently, in order to improve the three-dimensional model, more than 12 SD-OCT scans are needed, resulting in sectors smaller than 30°. A sector size of 1° or smaller would be ideal, but would increase the expenditure of time for the handmade measurements enormously. Even though Pro/ENGINEER is software widely used in professional engineering, there might be more suitable software on the market for this task.

Another possibility to improve the results of the present study would be an en face approach whereby the OCT device scans the eye frontally and not sagittally.[35,36]

The major limitation is the use of a fixed structure–function grid that was not individualized. The effect of the individual size, location, and tilt of the ONH was not respected in the present study. Thus, better correlations are likely to be achieved when an individualized measurement scheme and an individualized VF map for each patient are used.[3] This means that the axis between the fovea and the ONH should be respected and the SD-OCT images should have been oriented along this axis before the scans were recorded.[18,19,37] In some cases a neighboring VF sector showed high or even better correlation than the sector that was actually related to the compared distance or area. This phenomenon was observed when the structural parameters of the MD-NI VF sector (MRW-NI, PRW-NI, HRW-NI, MRA-NI, PRA-NI) were correlated with the MD-TI VF sector. This indicates that the VF sector grid should be rotated a few degrees counterclockwise (in right eye format).

With the present approach, Spearman's correlation coefficients up to $\rho = 0.77205$ between structure and function were observed within the patient group using new BMO-based parameters. In general, this suggests that BMO-based parameters are currently the most reasonable approach for structural measurements in glaucoma patients. In particular, it can be derived from the results of this study that the newly introduced PRW and PRA are equally or better correlated than MRW and MRA. Both findings lead closer to the underlying goal of early objective assessment of functional glaucomatous impairments.

Acknowledgments

The authors thank Michael S. Berger, who helped with his engineering expertise to design the CAD model of the neuroretinal rim.

Disclosure: **D.R. Muth**, None; **C.W. Hirneiß**, None

References

1. Quigley HA, Broman AT. The number of people with glaucoma worldwide in 2010 and 2020. *Br J Ophthalmol*. 2006;90:262–267.
2. Anderson RS. The psychophysics of glaucoma: improving the structure/function relationship. *Prog Retin Eye Res*. 2006;25:79–97.
3. Malik R, Swanson WH, Garway-Heath DF. "Structure-function relationship" in glaucoma: past thinking and current concepts. *Clin Experiment Ophthalmol*. 2012;40:369–380.
4. Weinreb RN, Khaw PT. Primary open-angle glaucoma. *Lancet*. 2004;363:1711–1720.
5. Ferreras A, Pablo LE, Garway-Heath DF, Fogagnolo P, Garcia-Feijoo J. Mapping standard automated perimetry to the peripapillary retinal nerve fiber layer in glaucoma. *Invest Ophthalmol Vis Sci*. 2008;49:3018–3025.
6. Gardiner SK, Johnson CA, Cioffi GA. Evaluation of the structure-function relationship in glaucoma. *Invest Ophthalmol Vis Sci*. 2005;46:3712–3717.
7. Johnson CA, Cioffi GA, Liebmann JR, Sample PA, Zangwill LM, Weinreb RN. The relationship between structural and functional alterations in glaucoma: a review. *Semin Ophthalmol*. 2000;15:221–233.
8. Bowd C, Zangwill LM, Medeiros FA, et al. Structure-function relationships using confocal scanning laser ophthalmoscopy, optical coherence tomography, and scanning laser polarimetry. *Invest Ophthalmol Vis Sci*. 2006;47:2889–2895.
9. Reus NJ, Lemij HG. Relationships between standard automated perimetry, HRT confocal scanning laser ophthalmoscopy, and GDx VCC scanning laser polarimetry. *Invest Ophthalmol Vis Sci*. 2005;46:4182–4188.
10. Medeiros FA, Alencar LM, Zangwill LM, Bowd C, Sample PA, Weinreb RN. Prediction of functional loss in glaucoma from progressive optic disc damage. *Arch Ophthalmol*. 2009;127:1250–1256.
11. Nilforushan N, Nassiri N, Moghimi S, et al. Structure-function relationships between spectral-domain OCT and standard achromatic perimetry. *Invest Ophthalmol Vis Sci*. 2012;53:2740–2748.
12. Chen TC. Spectral domain optical coherence tomography in glaucoma: qualitative and quantitative analysis of the optic nerve head and retinal nerve fiber layer (an AOS thesis). *Trans Am Ophthalmol Soc*. 2009;107:254–281.
13. Schlottmann PG, De Cilla S, Greenfield DS, Caprioli J, Garway-Heath DF. Relationship between visual field sensitivity and retinal nerve fiber layer thickness as measured by scanning laser polarimetry. *Invest Ophthalmol Vis Sci*. 2004;45:1823–1829.
14. Susanna R Jr, Vessani RM. Staging glaucoma patient: why and how? *Open Ophthalmol J*. 2009;3:59–64.
15. Denniss J, Henson D. The structure-function relationship in glaucoma: implications for disease detection. *Optom Pract*. 2009;10:95–104.
16. Schuman JS. Detection and diagnosis of glaucoma: ocular imaging. *Invest Ophthalmol Vis Sci*. 2012;53:2488–2490.
17. Pollet-Villard F, Chiquet C, Romanet JP, Noel C, Aptel F. Structure-function relationships with spectral-domain optical coherence tomography retinal nerve fiber layer and optic nerve head measurements. *Invest Ophthalmol Vis Sci*. 2014;55:2953–2962.
18. Chauhan BC, Burgoyne CF. From clinical examination of the optic disc to clinical assessment of the optic nerve head: a paradigm change. *Am J Ophthalmol*. 2013;156:218–227, e212.

19. Povazay B, Hofer B, Hermann B, et al. Minimum distance mapping using three-dimensional optical coherence tomography for glaucoma diagnosis. *J Biomed Opt*. 2007;12:041204.
20. Reis AS, Sharpe GP, Yang H, Nicolela MT, Burgoyne CF, Chauhan BC. Optic disc margin anatomy in patients with glaucoma and normal controls with spectral domain optical coherence tomography. *Ophthalmology*. 2012;119:738–747.
21. Chauhan BC, O'Leary N, Almobarak FA, et al. Enhanced detection of open-angle glaucoma with an anatomically accurate optical coherence tomography-derived neuroretinal rim parameter. *Ophthalmology*. 2013;120:535–543.
22. Hodapp E, Parrish RK, Anderson DR. *Clinical Decisions in Glaucoma*. 1st ed. St. Louis, MO: C. V. Mosby; 1993.
23. Kymes S. Cost-effectiveness of monotherapy treatment of glaucoma and ocular hypertension with the lipid class of medications. *Am J Ophthalmol*. 2006;142:354, author reply 354–355.
24. Naghizadeh F, Garas A, Vargha P, Hollo G. Structure-function relationship between the octopus perimeter cluster mean sensitivity and sector retinal nerve fiber layer thickness measured with the RTVue optical coherence tomography and scanning laser polarimetry. *J Glaucoma*. 2014;23:11–18.
25. Garway-Heath DF, Holder GE, Fitzke FW, Hitchings RA. Relationship between electrophysiological, psychophysical, and anatomical measurements in glaucoma. *Invest Ophthalmol Vis Sci*. 2002;43:2213–2220.
26. Weaver B, Wuensch KL. SPSS and SAS programs for comparing Pearson correlations and OLS regression coefficients. *Behav Res Methods*. 2013;45:880–895.
27. Wilcox RR, Tian T. Comparing dependent correlations. *J Gen Psychol*. 2008;135:105–112.
28. Diedenhofen B, Musch J. CoCor - Comparing Correlations. Available at: http://comparingcorrelations.org/. Accessed January 26, 2015.
29. Rolle T, Briamonte C, Curto D, Grignolo FM. Ganglion cell complex and retinal nerve fiber layer measured by fourier-domain optical coherence tomography for early detection of structural damage in patients with preperimetric glaucoma. *Clin Ophthalmol*. 2011;5:961–969.
30. Miglior S, Riva I, Guareschi M, et al. Retinal sensitivity and retinal nerve fiber layer thickness measured by optical coherence tomography in glaucoma. *Am J Ophthalmol*. 2007;144:733–740.
31. Leite MT, Zangwill LM, Weinreb RN, Rao HL, Alencar LM, Medeiros FA. Structure-function relationships using the Cirrus spectral domain optical coherence tomograph and standard automated perimetry. *J Glaucoma*. 2012;21:49–54.
32. Rao HL, Zangwill LM, Weinreb RN, Leite MT, Sample PA, Medeiros FA. Structure-function relationship in glaucoma using spectral-domain optical coherence tomography. *Arch Ophthalmol*. 2011;129:864–871.
33. Reus NJ, Lemij HG. The relationship between standard automated perimetry and GDx VCC measurements. *Invest Ophthalmol Vis Sci*. 2004;45:840–845.
34. Jonas JB, Budde WM, Panda-Jonas S. Ophthalmoscopic evaluation of the optic nerve head. *Surv Ophthalmol*. 1999;43:293–320.
35. Srinivasan VJ, Adler DC, Chen Y, et al. Ultrahigh-speed optical coherence tomography for three-dimensional and en face imaging of the retina and optic nerve head. *Invest Ophthalmol Vis Sci*. 2008;49:5103–5110.
36. Wolff B, Matet A, Vasseur V, Sahel JA, Mauget-Faysse M. En face OCT imaging for the diagnosis of outer retinal tubulations in age-related macular degeneration. *J Ophthalmol*. 2012;2012:542417.
37. Garway-Heath DF, Poinoosawmy D, Fitzke FW, Hitchings RA. Mapping the visual field to the optic disc in normal tension glaucoma eyes. *Ophthalmology*. 2000;107:1809–1815.

Investigative Ophthalmology & Visual Science